Segmenting Humeral Submovements using Invariant Geometric Signatures

Rakesh Krishnan [12], Niclas Björsell[2], and Christian Smith[1]

***Abstract*—Discrete submovements are the building blocks of any complex movement. When robots collaborate with humans, extraction of such submovements can be very helpful in applications such as robot-assisted rehabilitation. Our work aims to segment these submovements based on the invariant geometric information embedded in segment kinematics. Moreover, this segmentation is achieved without any explicit kinematic representation. Our work demonstrates the usefulness of this invariant framework in segmenting a variety of humeral movements, which are performed at different speeds across different subjects. Our results indicate that this invariant framework has high computational reliability despite the inherent variability in human motion.**

I. Introduction

Recent advances in robotics require humans and robots to interact at both physical and cognitive levels. Currently, in robot-assisted rehabilitation, this interaction design is a crucial factor that determines the success of this technology. Moreover, such a situation requires this interaction to be based on a computational structure that meets the challenge of high computational reliability [1]. Consequently, this mathematical framework must enable reliable perception of human intention, planning and assisting in task execution.

Despite this need at a kinematic level, a lack of agreement exists on a computational framework that can meet this challenge [2]. Similarly, when using kinematics to extract the neural policy, the choice of the kinematic representation results in conclusions that are coordinate sensitive [3], [4]. Importantly, many standard machine learning algorithms have been criticized for being coordinate sensitive [5]. A possible solution to this problem is the use of an invariant kinematic framework. The work presented in this paper is an important step in this direction. Through the present work, we aim to segment humeral submovements based on the invariant geometric information underlying the motion of interest (see Fig. 1).

Why is an invariant framework important? An invariant kinematic framework presents an unbiased perspective on the underlying neural computation [6]. Moreover, such knowledge of kinematic invariances

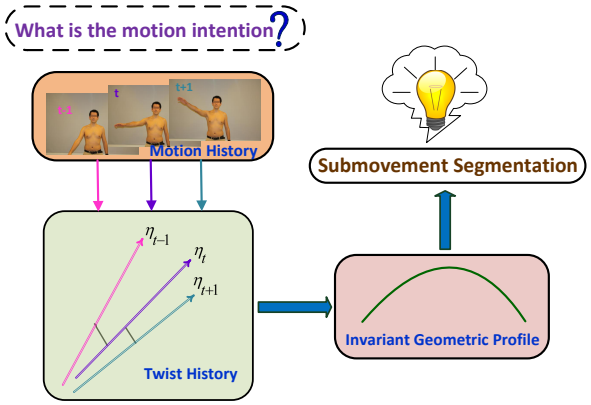

Figure 1: The central concept of invariant motion segmentation is presented above. This segmentation is achieved through an invariant geometric profile from the twist-axis history parameterizing the motion of interest.

can be helpful in reliable extraction of submovements. Essentially, these submovements are an integral part of human motion; they are of discrete nature [7]. It is hypothesized that the geometric information related to human intention is embedded in bone or segment motion [8]. Given this situation, we are motivated to explore this problem of segmenting human intention on the basis of segment kinematics.

In fact, the demands of this scientific problem pose several mathematical and practical challenges. First, to meet the high computational reliability requirement, the movement segmentation must be coordinate insensitive. A possible solution to this problem is a computational framework that is free of any explicit representation, which forms the core of our work. Second, reliable measurements of segment kinematics pose practical issues due to soft tissue artifacts (STAs) [9]. Additionally, the non-commutative nature of 3D kinematics and the variability inherent in human motion pose mathematical issues [7].

In this paper, we explore the performance of geometric invariants that could potentially be extended to intention segmentation, which is based on the invariant framework proposed by Schutter [10]. Thus far, this framework has not been investigated in the case of human motion. In our work, we explore the invariant geometric properties of the humeral segment. Importantly, the humeral segment acts as an end-effector to the shoulder articulation. This articulation has the largest

*This work was supported by the (AAL Call 6) AXO-SUIT project

[1] Robotics, Perception & Learning (RPL) and BioMEx Center, KTH (Royal Institute of Technology), Stockholm, Sweden rkth@kth.se

[2] Department of Electronics, Mathematics and Natural Sciences, University of Gävle, Gävle, Sweden

known range of motion (ROM) in the human body [11]; thus, it results in a variety of unique movements. Therefore, the set of possible motions for many other segments in the human body may be viewed as subsets of the motions of the humeral segment.

Our paper introduces the concept and presents a brief overview of kinematic invariances in Section II. Subsequently, we present the coordinate-free kinematic framework that is used to segment the submovements in Section III. The experimental design and data processing procedure used in our study is detailed in Section IV. We successfully demonstrate the effectiveness of the submovement classification using the invariant framework for a variety of humeral movements in Section V. We conclude our work by emphasizing the high reliability of this framework in classifying the submovements (see Section VI).

II. Kinematic Invariances

Geometrically, a mathematical formulation that provides a complete description of motion by using a minimal set of parameters can be defined as an *invariant framework* [12]. Importantly, invariant features provide insights into underlying neural control [12] and movement generating principles [9]. Notably, the property of invariance might hold irrespective of the speed of motion and muscle stiffness rescaling [12]. Mathematically, the invariants present a unifying framework in which analysis of both observed motion and motion generation can be performed [10].

These invariances have primarily been investigated in the case of rhythmic motor tasks. However, the originating principles underlying rhythmic and discrete movements might be different [9]. Therefore, investigating invariances in discrete movements is also important because it will enable both intra-subject and inter-subject comparisons of human upper limb kinematics [13]. Furthermore, such knowledge of kinematic invariants can be of immense help in robot-assisted rehabilitation, in which the reliability of cognitive human-robot interaction could be enhanced.

A. A Brief Overview of Kinematic Invariances

A major challenge in investigating invariances is their generalizability across a variety of movements [7]. Therefore, diverse invariances exist in the literature. First, invariances at a kinematic level during highly skilled tasks have been studied by Viviani et al. [14]. In this study, it was found that irrespective of the speed of writing an alphabet, the relative time ratios of important kinematic features remained well preserved. The recent study by Karklinsky et al. [15] on the rhythmic ellipse drawing task demonstrated that human hand kinematics follows the two-thirds power law. Although this study verified the property, the origins of this behavior are debatable [9]. Furthermore, this law cannot explain the motion of accompanying joints that in turn drives the hand motion [9].

Invariances in the form of submovements during arm reaching movements have been investigated by Berman et al. [7]. They suggested that most of the existing literature in extracting submovements is hypothesis driven. Note that such an extraction requires a pre-specified geometric arm model. Importantly, in the case of shoulder movements, it has been shown that the shoulder movement does not follow the convex-concave principle that underlies such geometric simplifications [16], [17]. Therefore, extracting submovements using the humeral kinematics needs to be explored further. Our work is an important step toward extracting submovements based on pure kinematic data, without the need for any explicit geometric model.

III. Invariant rigid body motion

The invariant geometric framework presented in [10] uses twist velocities. These geometric twists can effectively handle simultaneous rotations and translations [7]. In general, they are represented using 6D spatial vectors denoted by

$$\boldsymbol{\eta} = \begin{bmatrix} \boldsymbol{\omega} \\ \mathbf{v} \end{bmatrix} \tag{1}$$

Depending on the choice of the twist components, there are different types of geometric twists [11]. In this paper, we will use angular velocities referred to the body-fixed coordinate frame and the linear velocity of the center of mass (COM) of the rigid body. The use of these respective frames is motivated by the experimental ease with which these quantities can be estimated from the observed motion data.

Now, we briefly present the invariant geometric framework proposed by Schutter in [10]. Given a rigid body motion, six geometric invariants can be extracted using this framework. The first two invariants ω_1 and v_1 parametrize the instantaneous kinematics about the twist-axis, and they are defined as

$$\omega_1 = \boldsymbol{\omega} \cdot \mathbf{e_x} \tag{2}$$

and

$$v_1 = \mathbf{v} \cdot \mathbf{e_x}. \tag{3}$$

Here, $\mathbf{e_x}$ is the unit vector along the twist axis. Note that ω_1, v_1 and $\mathbf{e_x}$ are signed quantities. The next two invariants ω_2 and v_2 parametrize the first-order motion properties of the twist-axis, and they are defined as

$$\omega_2 = \frac{(\boldsymbol{\omega} \times \dot{\boldsymbol{\omega}})}{\|\boldsymbol{\omega}\|^2} \cdot \mathbf{e_y} \tag{4}$$

and

$$v_2 = \mathbf{e_y} \cdot \dot{\mathbf{p}}_{\perp}. \tag{5}$$

Here, $\mathbf{e_y} = \pm\frac{\boldsymbol{\omega}\times\dot{\boldsymbol{\omega}}}{\|\boldsymbol{\omega}\times\dot{\boldsymbol{\omega}}\|}$ and $\mathbf{p}_\perp = \frac{\boldsymbol{\omega}\times\mathbf{v}}{\|\omega\|^2}$. The second-order motion properties of the twist-axis are parametrized by ω_3 and v_3, and they are expressed as

$$\omega_3 = \frac{(\boldsymbol{\omega}\times\dot{\boldsymbol{\omega}})\times(\boldsymbol{\omega}\times\ddot{\boldsymbol{\omega}})}{\|(\boldsymbol{\omega}\times\dot{\boldsymbol{\omega}})\|^2}\cdot\mathbf{e_x} \tag{6}$$

and

$$v_3 = \mathbf{e_x}\cdot\dot{\mathbf{p}}_\perp - \dot{p}_\parallel. \tag{7}$$

Here, $\dot{p}_\parallel = -\frac{\mathbf{e_z}\cdot\dot{p}_\perp}{\omega_2}$, and the relationship between the unit vectors $\mathbf{e_z} = \mathbf{e_x}\times\mathbf{e_y}$ holds. Furthermore, it was shown in [10] that these parameters do indeed satisfy the concept of the invariant framework mentioned in Section II. Note that in our work, an algorithm to estimate these twist velocities is presented in Section IV-B. Now, we explore how this framework can be used in submovement segmentation.

A. Submovement Segmentation

The strength of the geometric framework presented above is that it enables us to compare movements at three different levels, namely, they are normalizations based on execution speed, motion amplitude and motion profile.

The first two level comparisons based on time and motion amplitude can be achieved by

$$\bar{\omega}_i(\bar{t}) = \frac{\omega_i(t)t_f}{\Theta} \quad i = 1,2,3 \tag{8}$$

and

$$\bar{v}_i(\bar{t}) = \frac{v_i(t)t_f}{L} \quad i = 1,2,3. \tag{9}$$

Here, if t_f is the final time in a given motion, then $\bar{t} = \frac{t}{t_f}$ is the dimensionless time. The amplitude normalization is achieved by the angular and linear scale magnitudes given by $\Theta = \int_0^{t_f}|\omega_1|dt$ and $L = \int_0^{t_f}|v_1|dt$. Note that the normalized invariants in (8) and (9) are dependent on the motion profile.

To normalize the invariants with respect to the motion profile, we need to compute the geometric degree of advancement, which is given by

$$\dot{\xi}(t) = w\frac{|\omega_1|}{\Theta_s} + (1-w)\frac{|v_1|}{L_s}, \quad 0 \le w \le 1. \tag{10}$$

Here, Θ_s and L_s are the user-defined angular and linear scaling factors, respectively, and w represents the scaling weight. Since the motion of the humeral segment is not purely rotational, we choose a value of $w = 0.5$ as in [10]. This choice results in the six dimensionless geometric invariants,

$$\Omega_i(\xi) = \frac{\omega_i(t(\xi))}{\dot{\xi}(t(\xi))}, V_i(\xi) = \frac{v_i(t(\xi))}{\dot{\xi}(t(\xi))}, \tag{11}$$

where $i = 1,2,3$. Applying the appropriate transformations presented in [10] to (11) results in $\bar{\Omega}_i(\bar{\xi})$ and $\bar{V}_i(\bar{\xi})$, which are the six dimensionless geometric invariants normalized with respect to the motion profile. The submovements can be extracted depending on the nature of these invariants computed from the motion of interest. Let us present the aspects of the experimental design of our study.

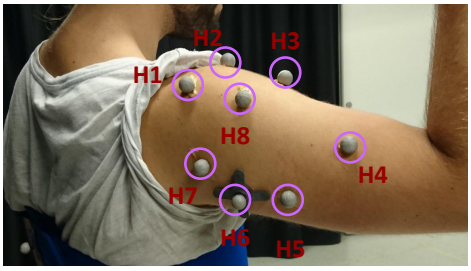

Figure 2: Figure illustrates the marker cluster for the humeral segment with labels H1-H8

IV. Measurements and Data Processing

This section begins with an overview of the experimental protocol, which is followed by the data processing method used to estimate the twist velocities. Subsequently, the humeral movements used in the study are presented.

A. Setup and Instructions

Six healthy subjects with fully functional upper arms were recruited (see Tab. I). Eight passive optical markers H1-H8 were attached on the humeral segment using double-sided tape (see Fig. 2) and were tracked using a 17-camera OptiTrack Motive motion capture system. The data were sampled at a rate of 120 fps (frames per second). The volunteers were instructed to perform five different movements in a standing position (see Section IV-C). Moreover, they were specifically instructed to minimize elbow and wrist motion when performing these tasks. Additionally, these movements were performed at different speeds (see Section IV-C). Estimating the twist velocities in (1) from the non-rigid marker cluster is a challenging problem, which we explore in the next subsection.

B. Estimating Twist Velocities from Non-rigid Marker Cluster

Computing the twist velocities in (1) from the surface marker cluster is an open problem. Therefore, mitigation of soft tissue artifacts is an important challenge that should be addressed before the geometric invariants can be analyzed. As a solution to this problem, we adapt the SHAPE algorithm presented in molecular dynamics [18]. The SHAPE algorithm is based on a non-Lagrangian approach; therefore, it is computationally less expensive compared to its Lagrangian counterparts.

Let $\mathbf{r_i}$ be the position coordinate of the ith particle of an n particle cluster with respective fictitious mass

m_i; then, the COM of the cluster is

$$\mathbf{r_{COM}} = \frac{\sum_{i=1}^{n} \mathbf{r_i} m_i}{\sum_{i=1}^{n} m_i} \tag{12}$$

To estimate the angular velocity, the coordinates of the ith particle are computed with respect to the COM by

$$\mathbf{r_i^b} = \mathbf{r_i} - \mathbf{r_{COM}} \tag{13}$$

The fictitious angular momentum of the particle cluster computed at the COM is given by

$$\mathbf{L^b} = \sum_{i=1}^{n} \mathbf{r_i^b} \times m_i \mathbf{v_i^b} \tag{14}$$

Note that the velocity $\mathbf{v_i^b}$ is computed from (13) using a forward difference approximation. If $\mathbf{r_i^b} \in \{x_i, y_i, z_i\}$ are the body-fixed coordinates of the ith particle, then the moment of inertia of the marker cluster is given by

$$\mathbf{I_b} = \begin{bmatrix} \sum m_i(y_i^2 + z_i^2) & -\sum m_i x_i y_i & -\sum m_i x_i z_i \\ -\sum m_i y_i x_i & \sum m_i(x_i^2 + z_i^2) & -\sum m_i y_i z_i \\ -\sum m_i z_i x_i & -\sum m_i z_i y_i & \sum m_i(x_i^2 + y_i^2) \end{bmatrix} \tag{15}$$

If δt is the data rate, by applying the law of conservation of angular momentum, the rigid angular velocity can be estimated by

$$\omega_{\mathbf{rigid}}^{\mathbf{b}}(t + \delta t/2) = {\mathbf{I_b}}^{-1} \mathbf{L_{non}}(t + \delta t/2) \tag{16}$$

Equation (16) is solved iteratively until the error norm is $||\mathbf{L_{non}^b} - \mathbf{L_{rigid}^b}|| < \epsilon$, where ϵ denotes a scalar positive tolerance. The readers are advised to refer to [18] for details regarding the implementation of this algorithm. The approximation error of the angular velocity estimate is on the order of δt^2. Note that this tolerance limit of ϵ can only be achieved by using eight humeral markers, and its convergence is dependent on the rate of deformation. The twist velocities in (1) are computed using (16) and (12).

C. Measurements

Our study is primarily based on naturalistic unconstrained arm motion, which is very challenging to investigate [19]. As mentioned in Section. III-A, we aim to segment the submovements from different stereotypical humeral movements performed under different speeds. Our hypothesis is that, irrespective of the speed of movement execution, we can segment the submovements, as the properties of the six dimensionless geometric invariants ($\bar{\Omega}_1 - \bar{\Omega}_3$, $\bar{V}_1 - \bar{V}_3$) depend only on the geometry of the motion being performed. Therefore, three basic shoulder movements in three different cardinal planes were selected. Initially, in the coronal plane, vertical abduction and adduction were chosen. During *abduction*, the humerus moves away from the midline of the body. When this movement is reversed, it results in *adduction*. When a similar movement is performed with reference to the transverse plane, it results in *horizontal abduction-adduction*. In the sagittal plane, when the humeral angle increases with respect to the thorax, it results in *flexion*. The reversal of this motion results in *extension*; when this reversal continues beyond the neutral position of the humerus, it results in *hyperextension*.

Table I: Details of healthy subjects involved in the study (F:Female, M:Male).

Subject	Age (years)	Weight (kg)	Height (m)	Handedness
1	25(F)	70	1.86	Right
2	24(M)	70	1.78	Right
3	32(M)	78	1.80	Right
4	24(F)	59	1.59	Right
5	21(M)	82	1.83	Right
6	25(M)	79	1.84	Right

Additionally, the above movements were performed with the help of a metronome at three different speeds, namely, ultra-slow (10 bpm (beats per minute)), slow (12 bpm), and normal (15 bpm), and without a metronome at a random (self-selected pace) speeds. The subjects were specifically instructed to finish the complete movement cycle in one beat cycle. Therefore, the transition times in the self-selected pace trials must demonstrate high variability. To ensure high quality of the recorded movements, the subjects were allowed to take short breaks in between various trials.

The above analysis was extended to two composite motion tasks performed at normal speed, in which each submovement occurred in different cardinal planes. The first task was *composite motion I*, which consisted of 90^o flexion followed by horizontal abduction and vertical adduction. Similarly, *composite motion II* begins with a vertical abduction of 90^o, followed by horizontal adduction and 90^o extension. All movements were repeated six times in each set.

V. Results and Discussion

This section begins with the analysis of the invariant geometric information for the five movements presented in Section IV-C. A video accompanying this submission emphasizes the relation between the geometric invariants and the various submovements of interest. In this section, these movements are analyzed using the mathematical framework presented in Section III and Section IV-B. The movements are presented in order of increasing number of submovements and complexity.

A. Vertical Abduction-Adduction

As illustrated in Fig. 3, from the humeral marker cluster, the twist velocities referred to the body-fixed frame are computed. From these estimated twist velocities, the six dimensionless geometric invariants can be extracted. Subsequently, by computing the geometric degree of advancement $\dot{\xi}(t)$, the six dimensionless geometric invariants are computed. The transition from the vertical abduction to adduction phase is marked by

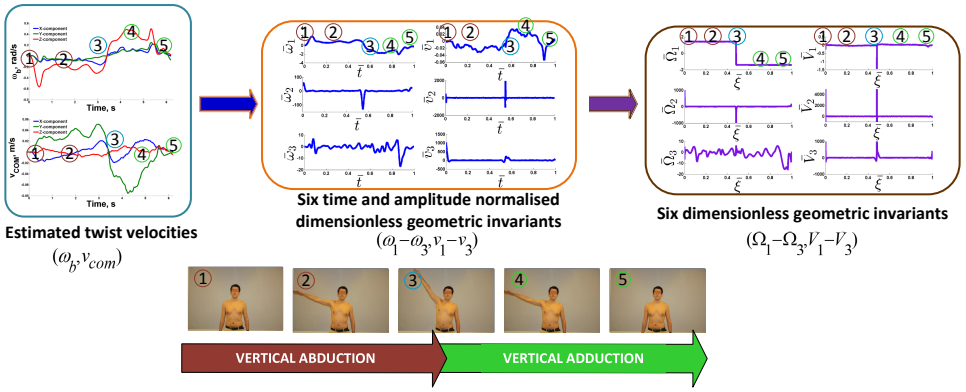

Figure 3: Representative illustration of extraction of invariant geometric signatures for Subject 2 during vertical abduction-adduction task performed at ultra-slow speed for a single cycle. From the estimated rigid body twist velocities $\boldsymbol{\omega_b}$ and $\mathbf{v_{COM}}$, the six time and amplitude normalized invariants are computed $\bar{\omega}_1 - \bar{\omega}_3$ and $\bar{v}_1 - \bar{v}_3$. Following this extraction, the six geometric invariants with respect to motion profile are computed $\bar{\Omega}_1 - \bar{\Omega}_3$ and $\bar{V}_1 - \bar{V}_3$. We follow the exact steps as detailed in [10].

the transition in sign of $\bar{\omega}_1$, which is accompanied by an instantaneous peak in $\bar{v}_1$. Corresponding changes can also be observed in the higher order invariants.

Similarly, the final set of invariants with respect to the motion profile $\bar{\Omega}_1$ and $\bar{V}_1$ also exhibit marked transitions. Corresponding changes can also be observed in the higher order invariants. Note that the higher the derivative level of the invariant descriptor is, the more sensitive the interpretation is to noise [20]. Therefore, we will henceforth use $\bar{\Omega}_1$ and $\bar{V}_1$ to segment the submovements.

As shown in Fig. 4, it is clear that by using the geometric invariants, it is possible to reliably segment the submovements at different speeds. The transition from vertical abduction to adduction is clearly marked by the transition from a positive to negative region of $\bar{\Omega}_1$ and the instantaneous trigger in $\bar{V}_1$. Note the high instantaneous linear velocity effect in Fig. 4. Such an effect in the invariants occurs when the subject attempts to complete a submovement in a shorter time than usual. This is accompanied by a high instantaneous linear velocity during execution of the submovement, which has also been reported by other studies [14].

B. Horizontal Abduction-Adduction

As shown in Fig. 5, during the horizontal abduction-adduction task, the change from horizontal abduction to adduction is marked by a clear change in the sign of $\bar{\Omega}_1$ and an event trigger in the plots of $\bar{V}_1$.

C. Flexion-Extension-Hyperextension

As shown in Fig. 6, the change from flexion to extension-hyperextension and the reversal of hyperextension are clearly marked by transitions in the value of $\bar{\Omega}_1$ and two event detectors in $\bar{V}_1$. We note here that, the reversal of motion from hyperextension to reverse hyperextension is accompanied by STA effects. This might be due to large acceleration of the marker cluster during this instantaneous reversal. As we previously mentioned (see Section. IV-B), the SHAPE algorithm has limitations handling large rates of deformations. Therefore, improving the algorithm would be a possible solution to mitigate these effects.

D. Composite Motions I & II

As shown in Fig.7, composite motions I and II are both accompanied by two clear transitions. During composite motion I, the changes from flexion to horizontal abduction and from horizontal abduction to vertical adduction are marked by clear transitions in the values of $\bar{\Omega}_1$ and $\bar{V}_1$. The invariants for composite motion II are also similar.

To further elucidate our analysis, we plot the relative submovement transition times for the various movements in Fig. 8. Note that in the case of both vertical and horizontal abduction-adduction only a single submovement transition time exists. Whereas, in the case of flexion-extension-hyperextension, the change from flexion to extension and hyperextension to reverse hyperextension is marked by two different transion times as seen in third column of Fig. 8. In general, the standard deviation of submovement transition time during the self-paced trial (case 4) is seen to be greater than other cases. This is not surprising as the subjects were specifically instructed to randomly select the submovement transition time (see Section IV-C). Therefore, the standard deviations of the submovement transition times demonstrate the high reliability of our submovement segmentation.

Interestingly, despite the approximate estimation of twist velocities from the marker cluster, we are able to segment the submovements with high reliability. Of course, improving the twist velocity estimation algorithm is key to the full exploitation of this invariant geometric framework. Currently, the invariant geometric framework presented in this paper is computed offline. Extending this framework to online implementation is

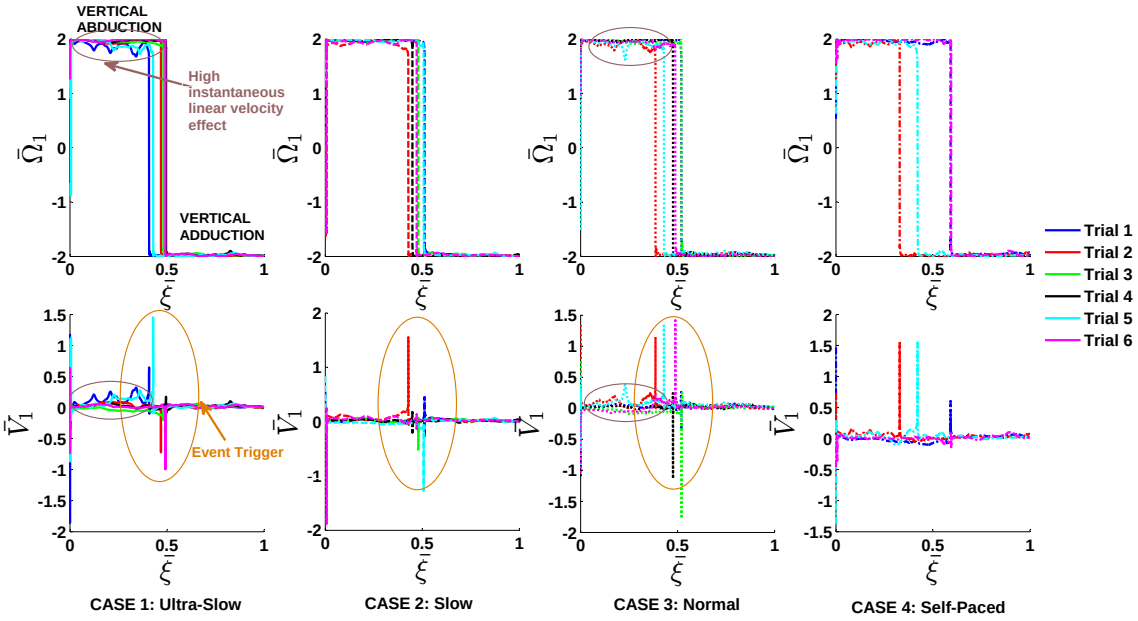

Figure 4: Representative dimensionless invariants $\bar{\Omega}_1$ and $\bar{V}_1$ for Subject 2 during vertical abduction-adduction task: ultra-slow (solid), slow (dashed), normal (dotted) and self-paced (dash-dotted)

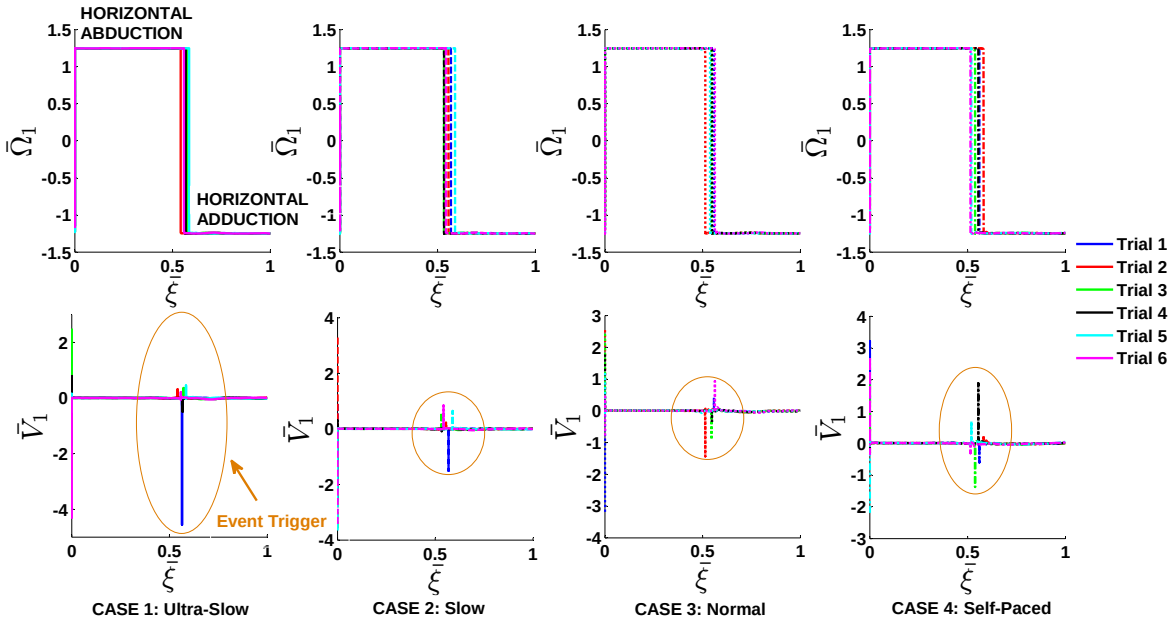

Figure 5: Representative dimensionless invariants $\bar{\Omega}_1$ and $\bar{V}_1$ for Subject 3 during horizontal abduction-adduction task: ultra-slow (solid), slow (dashed), normal (dotted) and self-paced (dash-dotted)

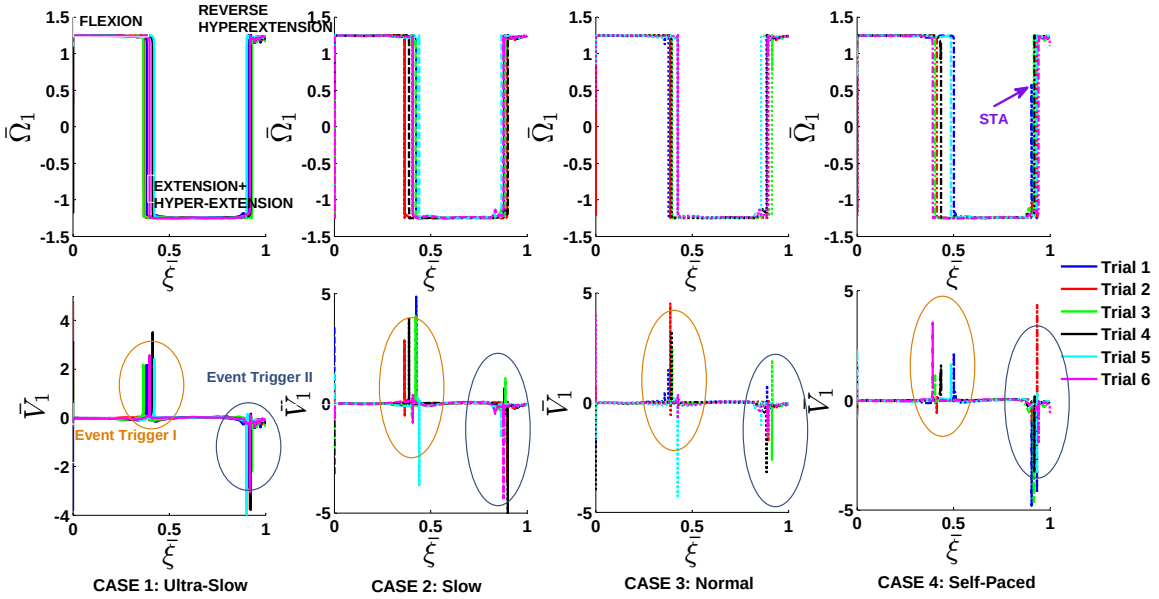

Figure 6: Representative dimensionless invariants $\bar{\Omega}_1$ and $\bar{V}_1$ for Subject 5 during flexion-extension-hyperextension task: ultra-slow (solid), slow (dashed), normal (dotted) and self-paced (dash-dotted)

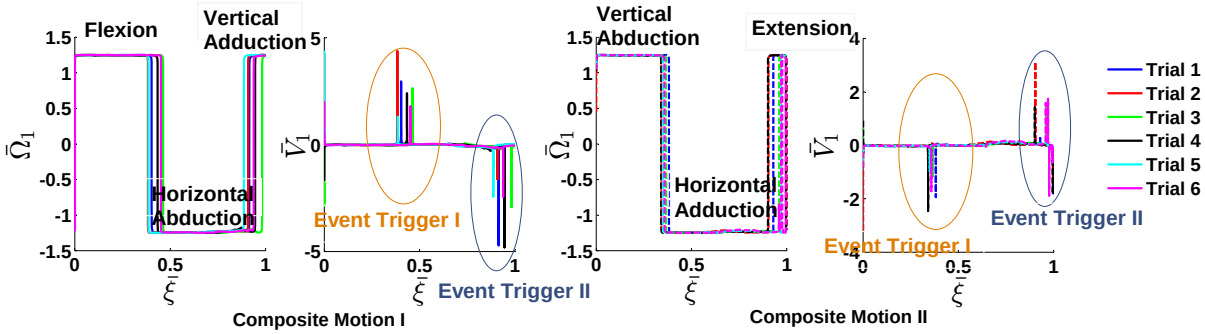

Figure 7: Figure illustrates the geometric invariants $\bar{\Omega}_1$ and $\bar{V}_1$ for composite Motion I (solid) and composite Motion II (dashed) for Subject 1 at a normal speed.

an important question that we would like to explore further. This framework would be very useful in applications such as high-intensity repetitive robot-assisted therapy. In the future, high-reliability HRI would require an invariant framework that would enable seamless communication between humans and robots. This work is an important step in this direction.

VI. Conclusions

Through this paper, we have successfully demonstrated that solely based on the invariant geometric information embedded in the segment kinematics, it is possible to segment the submovements with high reliability. This approach has been successfully tested across diverse naturalistic humeral movements, at different externally cued and self-selected speeds. In conclusion, the presented framework has high reliability of submovement segmentation for a large variety of movements. This consistent segmentation is achieved despite the inherent variability in the observed movements.

Acknowledgments

We thank Tamar Flash for the useful early discussion. We also acknowledge the subjects who volunteered for the study.

References

[1] J. Pons, "Rehabilitation exoskeletal robotics," *IEEE Eng. Med. Biol. Mag.*, vol. 29, no. 3, pp. 57–63, 2010.

[2] N. Jarrassé *et al.*, "Robotic Exoskeletons: A Perspective for the Rehabilitation of Arm Coordination in Stroke Patients," *Front. Hum. Neurosci.*, vol. 8, no. December, pp. 1–13, 2014.

[3] M. D. Klein Breteler and R. G. J. Meulenbroek, "Modeling 3D object manipulation: Synchronous single-axis joint rotations?" *Exp. Brain Res.*, vol. 168, no. 3, pp. 395–409, 2006.

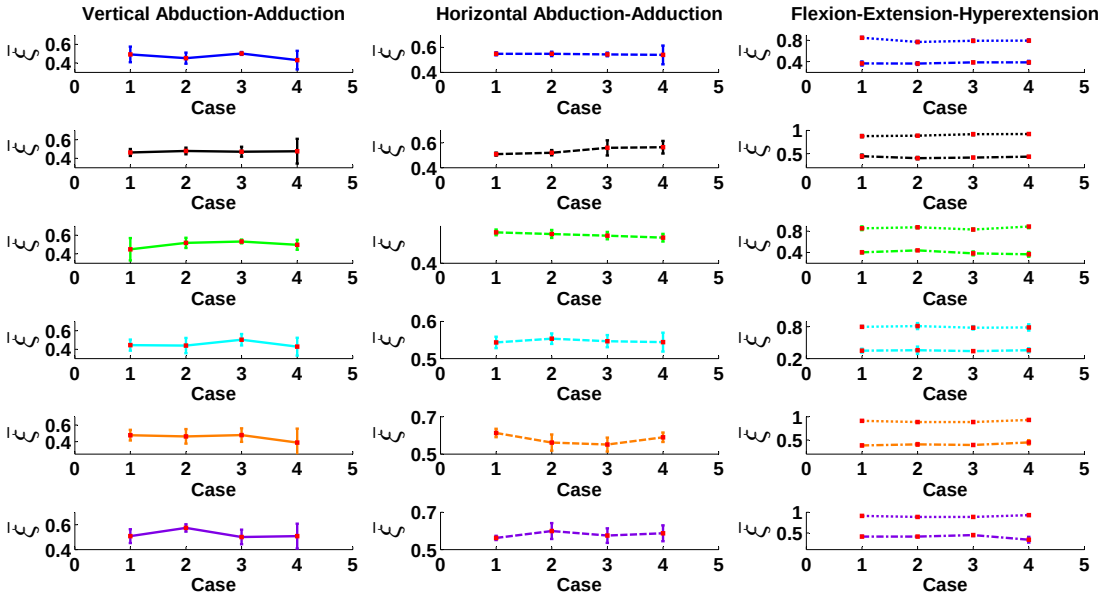

Figure 8: Plot of mean and standard deviation of submovement transition time $\bar{\xi}$ for different submovements, namely: vertical abduction-adduction (solid), horizontal abduction-adduction (dashed), flexion-extension (dot-dashed), hyperextension- reverse hyperextension (dotted). Each row represents subjects 1-6 in the respective order as in Tab. I. In each sub-plot, the cases 1-4 represent the ultra-slow, slow, normal and self-paced trials.

[4] D. Sternad *et al.*, "Coordinate Dependence of Variability Analysis," *PLoS Comput. Biol.*, vol. 6, no. 4, p. e1000751, apr 2010.

[5] D. Campolo *et al.*, "Analysis of Accuracy in Pointing with Redundant Hand-held Tools: A Geometric Approach to the Uncontrolled Manifold Method," *PLoS Comput. Biol.*, vol. 9, no. 4, 2013.

[6] D. Hestenes, "Invariant Body Kinematics .1. Saccadic and Compensatory Eye-Movements," *Neural Networks*, vol. 7, no. 1, pp. 65–77, 1994.

[7] S. Berman *et al.*, "Application of motor algebra to the analysis of human arm movements," *Robotica*, vol. 26, no. 04, pp. 435–451, 2008.

[8] L.S. Lippert, *Clinical Kinesiology and Anatomy*, 5th ed. F. A. Davis Company, 2011.

[9] S. Schaal and D. Sternad, "Origins and violations of the 2/3 power law in rhythmic three-dimensional arm movements," *Exp. Brain Res.*, vol. 136, no. 1, pp. 60–72, 2001.

[10] J. De Schutter, "Invariant Description of Rigid Body Motion Trajectories," *J. Mech. Robot.*, vol. 2, no. 1, p. 011004, 2010.

[11] R. Krishnan *et al.*, "Invariant spatial parametrization of human thoracohumeral kinematics: A feasibility study," in *2016 IEEE/RSJ Int. Conf. Intell. Robot. Syst.* IEEE, oct 2016, pp. 4469–4476.

[12] D. Hestenes, "Invariant body kinematics: II. Reaching and neurogeometry," *Neural Networks*, vol. 7, no. 1, pp. 79–88, jan 1994.

[13] G. Rau *et al.*, "Movement biomechanics goes upwards: From the leg to the arm," *J. Biomech.*, vol. 33, no. 10, pp. 1207–1216, 2000.

[14] P. Viviani and C. Terzuolo, "Space-time invariance in motor skills," in *Tutorials Mot. Behav.*, 1980, pp. 525–533.

[15] M. Karklinsky and T. Flash, "Timing of continuous motor imagery: the two-thirds power law originates in trajectory planning," *J. Neurophysiol.*, vol. 113, no. 7, pp. 2490–2499, 2015.

[16] J. Schomacher, "The convex–concave rule and the lever law," *Man. Ther.*, vol. 14, no. 5, pp. 579–582, 2009.

[17] B. Tondu, "Estimating shoulder-complex mobility," *Appl. Bionics Biomech.*, vol. 4, no. 1, pp. 19–29, 2007.

[18] P. Tao *et al.*, "Maintain rigid structures in Verlet based Cartesian molecular dynamics simulations," *J. Chem. Phys.*, vol. 137, no. 13, 2012.

[19] J. N. Ingram and D. M. Wolpert, "Naturalistic approaches to sensorimotor control," in *Prog. Brain Res.*, 2011, vol. 191, pp. 3–29.

[20] M. Vochten *et al.*, "Comparison of rigid body motion trajectory descriptors for motion representation and recognition," in *2015 IEEE Int. Conf. Robot. Autom.* IEEE, may 2015, pp. 3010–3017.